Published on “Earth and Planetary Science Letters”, 450 (2016) 292–30

Origin and role of fluids involved in the seismic cycle of extensional faults in carbonate rocks

Luca Smeraglia [a], Fabrizio Berra [b], Andrea Billi [c], Chiara Boschi [d], Eugenio Carminati [a,c], Carlo Doglioni [a,c]

[a] *Dipartimento di Scienze della Terra, Sapienza Università di Roma, P.le Aldo Moro 5, 00185 Roma, Italy* [b] *Università degli Studi di Milano, Dipartimento di Scienze della Terra, Via Mangiagalli 34, 20133 Milano, Italy* [c] *Consiglio delle Nazionale Ricerche, IGAG, c.o. Dipartimento di Scienze della Terra, Sapienza Università di Roma, P.le Aldo Moro 5, 00185 Roma, Italy* [d] *Istituto di Geoscienze e Georisorse, Consiglio Nazionale delle Ricerche, Via Moruzzi 1, 56124 Pisa, Italy*

Keywords: fluid circulation seismic cycle fluid pressure stable isotopes fault zone evolution central Apennines

ABSTRACT

We then used C- and O-isotope data from different generations of fault-related mineralizations to show a shift from connate (marine-derived) to meteoric fluid circulation during exhumation from 3 to ≤1 km depths and concurrent fluid cooling from ∼68 to <30◦C. Between ∼3 km and ∼1 km depths, impermeable barriers within the sedimentary sequence created a semi-closed hydrological system, where prevalently connate fluids circulated within the fault zone at temperatures between 60◦ and 75 ◦C. During fault zone exhumation, at depths ≤1 km and temperatures <30 ◦C, the hydrological circulation became open and meteoric-derived fluids progressively infiltrated and circulated within the fault zone. The role of these fluids during syn-exhumation seismic cycles of the Tre Monti Fault has been substantially passive along the whole fault zone, the fluids being passively redistributed at hydrostatic pressure following co-seismic dilatancy. Only the principal fault has been characterized, locally and transiently, by fluid overpressures. The presence of low-permeability clayey layers in the sedimentary sequence contributed to control the type of fluids infiltrating into the fault zone and possibly their transient overpressures. These results can foster the comprehension of seismic faulting at shallow depths in carbonate rocks of other fold-thrust belts involved in post-collisional seismogenic extensional tectonics. We examine the potentially-seismic right-lateral transtensional–extensional Tre Monti Fault (central Apennines, Italy) with structural and geochemical methods and develop a conceptual evolutionary model of extensional faulting with fluid involvement in shallow (≤3 km depth) faults in carbonate rocks. In the analysed fault zone, multiscale fault rock structures include injection veins, fluidized ultracataclasite layers, and crackle breccias, suggesting that the fault slipped seismically. We reconstructed the relative chronology of these structures through cross-cutting relationship and cathodoluminescence analyses.

1. Introduction

Fluid flow along faults has been widely explored for implications on various topics including hydrocarbon and ore exploration, CO_2 sequestration, groundwater and contaminant transport, and faulting (e.g., Cox, 1995; Williams et al., 2015). Faults and fault zones can be preferential conduits or barriers for the passage of geofluids. Moreover, fault slip behaviors and the seismic cycle are often controlled by the geofluids themselves (e.g., Hickman et al., 1995).

Fluids have been suggested to play either passive or active roles during the seismic cycle (e.g., Sibson, 2014; Fig. 1). For instance, the “fault-valve” model (Fig. 1a) involves an active role of overpressured fluids that can trigger earthquakes (e.g., Miller et al., 2004; Haney et al., 2005). After seismic failure, fluid discharge and sealing mineralizations are favored by hydrofracturing and decompression (stress drop), respectively (e.g., Cox, 1995). Complete fracture sealing allows fluid overpressure to build again and initiate a new seismic cycle. This mechanism can commonly act within fluid-overpressured crustal blocks (e.g., Di Luccio et al., 2010), especially along subduction interfaces, where fluid overpressure is more likely to develop and be sustained (Sibson, 2014). On the other hand, different scenarios involve a passive role of fluids that are redistributed following an earthquake (e.g., Sibson, 2000).

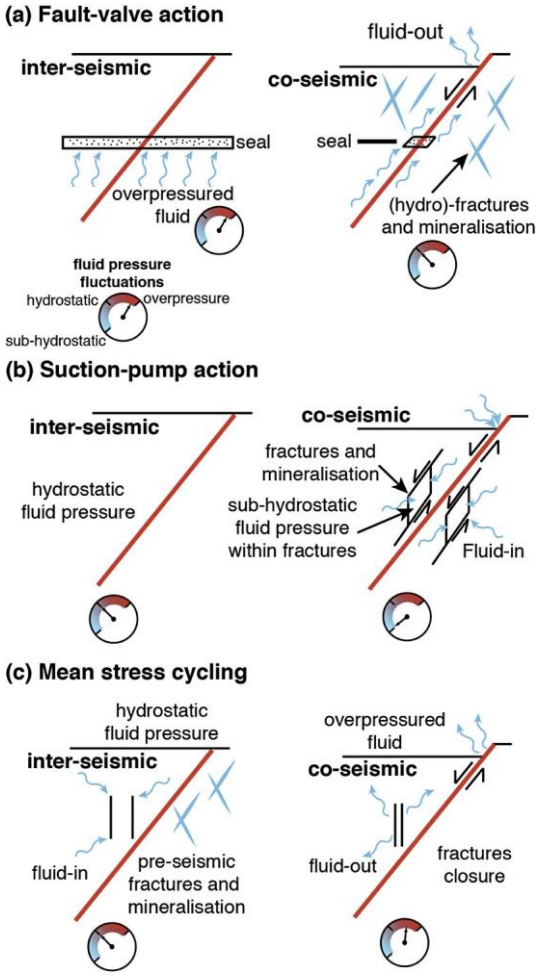

Fig. 1. Different models of interaction between fluids and seismic cycles (modified after Sibson, 2000). (a) Fault-valve action. (b) Suction-pump action. (c) Mean stress cycling.

Fluid redistribution can be favored by rapid co-seismic dilation and creation of high-permeability fracture networks characterized by subhydrostatic pressure (Fig. 1b, "suction-pump" model) or by crack closure favored by post-seismic stress recovery (Fig. 1c, "mean stress cycling" model). If low-permeability barriers are not created, fluids conserve hydrostatic pressure. These mechanisms can easily act within extensional/transtensional regimes (e.g., Doglioni et al., 2014; Sibson, 2014) in the shallow crust (<5 km), where hydrostatic fluid pressure and high permeability zones have been documented (Townend and Zoback, 2000). These processes can be understood and validated by studying the evidence of seismicrelated mineralization and rock-related fluid structures and textures (e.g., Uysal et al., 2009; Rowe and Griffith, 2015). Therefore, the study of the geological record of fluid–fault interactions is a fundamental pre-requisite for general models concerning the origin and role of fluids involved in the seismic cycle. Single case histories are fundamental to build comprehensive conceptual models of seismic-related fluid circulation.

We examine a case study of a major right-lateral transtensional– extensional fault (Tre Monti Fault, TMF, central Apennines, Italy) from a carbonate domain in the central Apennines, Italy (Fig. 2a). The study of this fault is relevant as, at shallow crustal levels (<10 km depth), fault zones in carbonate rocks represent favorable structures for migration and entrapment of geofluids (e.g., Ghisetti et al., 2001). Moreover, in many seismically active regions worldwide (including our study area), shallow crustal earthquakes and seismic sequences (e.g., hypocenters at <10 km depth) nucleate in and propagate upward through carbonate rocks with fluids involvement in the seismic cycle (e.g., Macedonia, Greece, 1995, M_w 6.6 earthquake, Stiros, 1995; Wenchuan, China, 2008, M_w 8.0 earthquake, Chen et al., 2013; L'Aquila, Italy, 2009, M_w 6.3 earthquake, Chiaraluce, 2012).

The TMF has been exhumed from depths ≤3 km since about the Pliocene (Galadini et al., 2003) and exhibits excellent exposures allowing geoscientists to study the relationships between fault zone architecture, fluid circulation, and seismic cycle within a tectonically active extensional setting (Smith et al., 2011). As many normal fault earthquakes frequently cause surface ruptures and associated damage and fatalities (Stiros, 1995; Galli et al., 2008), the study of such a shallow fault is relevant for the understanding of the fault zone architecture and fluid circulation at shallow depths (≤3 km).

We synthesize the spatio-temporal tectonic evolution and fluid circulation of the TMF into a conceptual model of seismic-related fluid circulation within shallow (≤3 km) extensional fault zones. We combine structural, microstructural, mineralogical, and

geochemical (cathodoluminescence, stable isotopes, and whole rock geochemistry) methods. The main novelty of this model concerns the origin of geofluids involved in the seismic cycle of exhuming extensional fault zones and their specific role, which is substantially passive along most part of the fault zone except along the principal fault, where fluid overpressures can locally arise during co-seismic phases.

2. Geological setting

2.1. *Apennines evolution and seismotectonic setting*

The Central Apennines is a late Oligocene-to-Present fold-andthrust belt related to the west directed subduction and eastward rollback of the Adriatic plate under the European plate (Doglioni, 1991). Shortening was characterized by the northeastward migration of thrust fronts in a classical forelandward piggy-back sequence of thrust sheets (Cosentino et al., 2010). These tectonic processes juxtaposed carbonates onto syn-orogenic deposits along NW-SE-oriented thrust faults (Fig. 2a; Cosentino et al., 2010). The thrust sheets consist of ∼4–5 km thick Late Triassic–Middle Miocene shallow-water carbonate rocks, whereas the syn-orogenic deposits consist of up to ∼3 km thick Late Miocene hemipelagic marls and deep-marine siliciclastic sandstones with intercalated clayey layers (Cosentino et al., 2010).

Since Late Miocene time, while the compressional deformation was still active along the eastern fronts (Adriatic domain), the Apennines belt experienced extension and exhumation in its western and axial parts. This process has been associated with exhumation at rates of ca. 0.3 mm/a in the last 3–5 Ma (e.g., Thomson et al., 2010 for the Northern Apennines). Normal faulting led to crustal thinning related to the development of the Tyrrhenian backarc basin (Doglioni, 1991). This process is still active and has generated a system of NW-SE-oriented basin-bounding active extensional faults and perpendicular strike- to oblique-slip transfer faults (Fig. 2a). Both sets of faults produced large historical and instrumental earthquakes up to M_w 7 (Fig. 2a; e.g., Avezzano, 1915, M_w 7.0 earthquake; L'Aquila, 2009, M_w 6.3 earthquake; Galli et al., 2008; Chiaraluce, 2012). The TMF represents an active or recently-active transfer fault between two NW-SE-oriented extensional faults (Morewood and Roberts, 2000; Benedetti et al., 2013).

In the Apennines, the imbricated carbonates and syn-orogenic sequences can be traced from the surface to depths of ca. 8–10 km (Patacca et al., 2008).

Although some mainshocks probably nucleated within the underlying crystalline basement (∼10 km depth), it is well documented that many foreshocks and aftershocks as well as some mainshocks nucleated and propagated within the overlying sedimentary sequence (Miller et al., 2004; Ventura and Di Giovambattista, 2013). Moreover, fluid–earthquake interactions at different crustal levels have been instrumentally documented for the most recent earthquakes of the region. For instance, near lithostatic fluid pressure at hypocentral depths triggered both the mainshocks and the aftershocks during the M_w 6.0, 1997 Colfiorito (Miller et al., 2004) and M_w 6.3, 2009 L'Aquila (Di Luccio et al., 2010) earthquakes. Malagnini et al. (2012) suggested that, during the L'Aquila earthquake, pore fluid pressure diffusion was responsible for the spatial migration of seismicity with the activation of different fault segments.

In the Apennines, earthquakes frequently ruptured the Earth's surface (e.g., Galli et al., 2008; Benedetti et al., 2013). Consequently, the fluids that circulate at shallow crustal levels (<1 km depth) can enter into and interact with the fault zone, as was the case, for instance, of the L'Aquila earthquake (Amoruso et al., 2011; Doglioni et al., 2014).

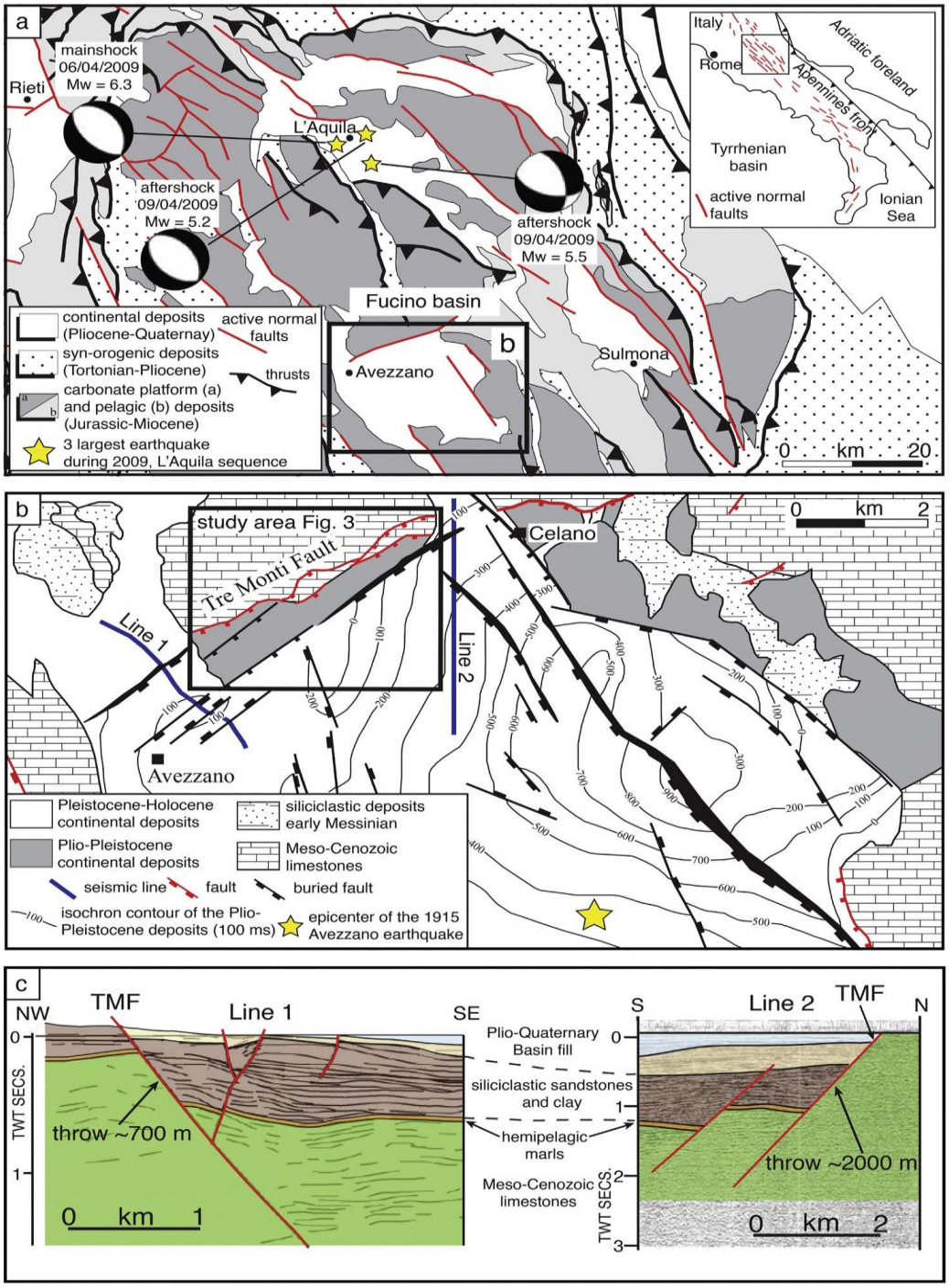

Fig. 2. (a) Simplified geological map of the central Apennines (Italy), showing main thrusts and active normal faults. Inset shows a schematic tectonic setting of centralsouthern Italy with main thrusts and active normal faults. (b) Geological setting of the Fucino basin and Tre Monti Fault (TMF) (Cavinato et al., 2002). (c) Seismic reflection cross-sections (left cross-section: data line drawing and interpretation; right cross-section: data and interpretation) through the TMF (Cavinato et al., 2002; Patacca et al., 2008). Cross-section traces are shown in (b).

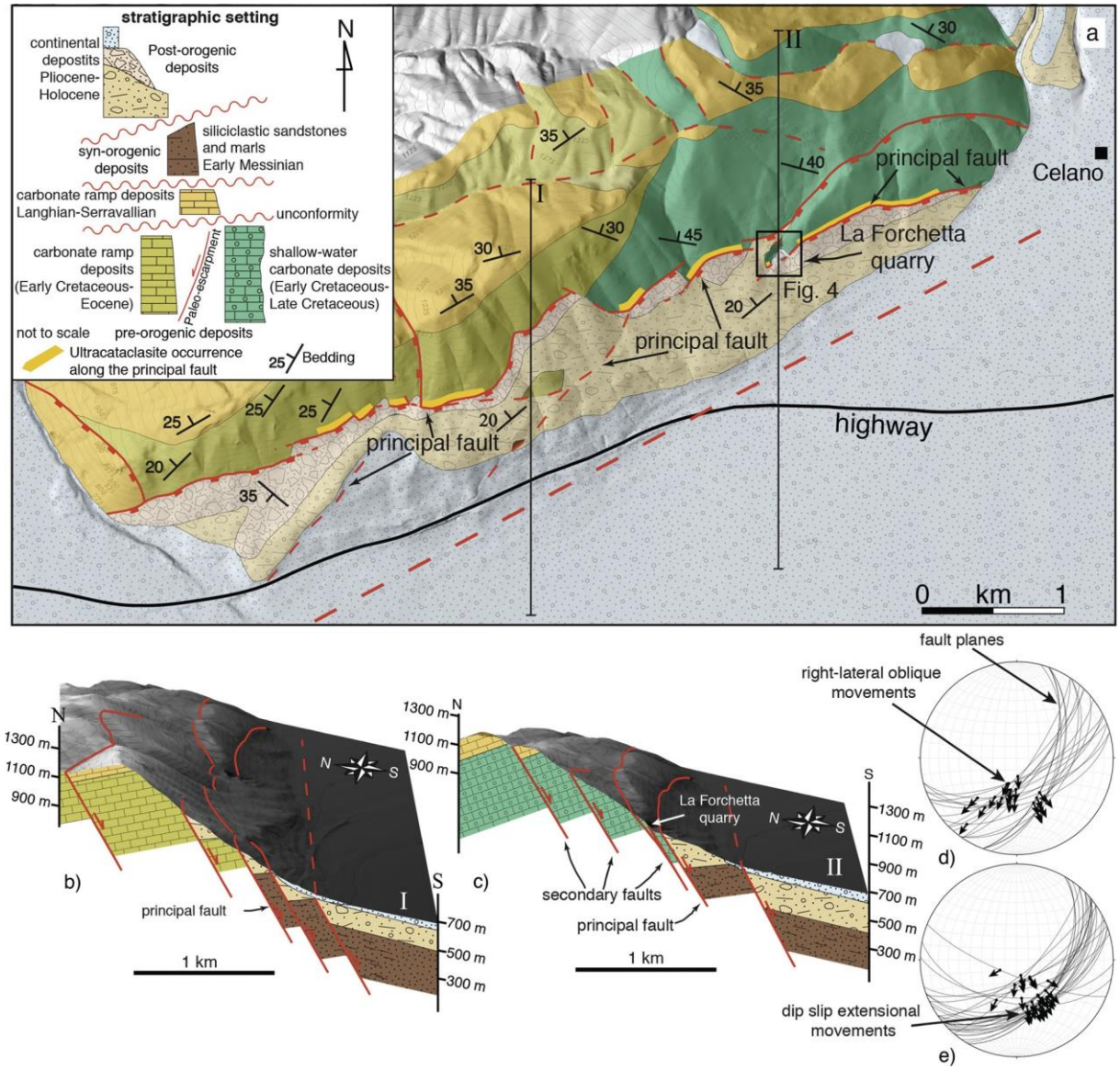

Fig. 3. (a) Geological map of the TMF area along the northern boundary of the Fucino basin. Inset shows the stratigraphic-structural relationships in the area. (b) and (c) Geological cross-sections through the TMF and topographic renditions of the Tre Monti Hills. Cross-section traces in (a). (d) Schmidt net (lower hemisphere) showing attitude of meso-scale fault surfaces and related slip vectors (right-lateral transtensional movements). (e) Schmidt net (lower hemisphere) showing attitude of meso-scale fault surfaces and related slip vectors (dip-slip extensional movements).

2.2. *The Tre Monti Fault*

The TMF marks the north-western boundary of the Fucino basin, which is an intra-mountain half-graben filled by Late Pliocene–Quaternary continental deposits (Fig. 2b; Cavinato et al., 2002). Paleoseismological investigations suggest that the TMF has been active between Early Pliocene and recent times (Benedetti et al., 2013). The TMF is exposed for a length of ~8 km along the southern slope of the Tre Monti Hills as an almost continuous series of ENE-WSW-oriented and SSE-dipping fault surfaces and scarps in Mesozoic limestones (Fig. 2b).

Based on stratigraphic offset and kinematic indicators, the TMF can be defined as an extensional fault with a transtensional rightlateral slip component (e.g., Morewood and Roberts, 2000). Seismic cross-sections through the TMF indicate that the cumulative throw increases from ~0.7 km in the western part to ~2 km in the eastern part (Fig. 2c, Cavinato et al., 2002; Patacca et al., 2008).

The TMF displaces the Tre Monti anticline, an open fold of Mesozoic–Cenozoic limestones and Late Tertiary syn-orogenic deposits with a north-western periclinal termination (Fig. 3a). The pre-orogenic carbonates crop out for a thickness of ~600 m and are unconformably overlain by syn-orogenic deposits with a minimum thickness of ~150 m (Fig. 3a). Vitrinite reflectance data indicate that, in this area, the syn-orogenic deposits were buried to maximum depths of up to 2 km (Corrado et al., 2010). As the tectonic activity of the TMF started both after the compressional deformation and after the deposition of syn-orogenic deposits, we infer that the exposed portion of the TMF was exhumed from depths ≤3 km.

3. Methods

We used the following methods to unravel the TMF architecture and fault-related fluid circulation:

(1) Original field mapping (at 1:5000 scale or larger) to reconstruct the TMF surface kilometric-scale geometry;

(2) Construction of two geological cross-sections through the TMF to calculate fault displacements and investigate the buried structure. The sections are constrained by field and seismic reflection data;

(3) Detailed structural analyses and systematic sampling within La Forchetta quarry to reconstruct the fault zone internal architecture;

(4) Analysis of fault-rock microstructures using optical microscopy to investigate the deformation mechanisms;

(5) X-ray diffraction analyses (XRD) to determine fault rock mineralogy;

(6) Cathodoluminescence microscopy (CL) employing a cold cathode luminoscope (Nuclide ELM2) to distinguish the different phases of fluid-related mineralizations;

(7) Stable isotope analyses using a mass spectrometer (Finnigan MAT Delta Plus) equipped with Finnigan Gas-Bench II at the Institute of Geosciences and Earth Resources (IGG, CNR, National Research Council, Pisa, Italy). The experimental values were normalized against international (NBS-18) and internal standards. We verified a mean external reproducibility better than 0.1 both for $\delta^{13}C$ and for $\delta^{18}O$. Results are reported according to the conventional δ notations Vienna Pee Dee Belemnite (PDB) and Vienna Standard Mean Ocean Water (SMOW);

(8) Whole fault rock chemical analyses through an inductively coupled plasma-mass spectrometry (ICP-MS) at the Actlabs research laboratories (www.actlabs.com).

(9)

4. Structural and cathodoluminescence data

4.1. Fault zone setting and general architecture

The TMF is segmented into up to eleven SSE-dipping (45◦–65◦) fault segments (Fig. 3a). A buried fault segment occurs at the foot of the Tre Monti hills as inferred by seismic reflection data (Cavinato et al., 2002; Fig. 3a). The principal fault surface coincides with the most downhill fault scarp, and juxtaposes carbonate rocks in the footwall with both syn-orogenic marine and post-orogenic continental deposits in the hangingwall (Figs. 3b and 3c). The latter deposits consist of subaerial slope debris composed by carbonate clasts cemented by calcite precipitates.

The principal fault is exposed along a series of en-échelon parallel fault scarps, whereas other segments are buried and inferred by morphological evidence (scarps interpreted as tectonicallycontrolled) within the continental deposits (Fig. 3a). The principal fault surfaces are commonly striated by sets of slickenlines indicating two main movements: transtensional right-lateral (Fig. 3d) and extensional dip-slip (Fig. 3e). We observed no overprinting relationships between slip indicators. A set of secondary synthetic faults is hosted in the carbonate bedrock behind the principal fault (Figs. 3b and 3c). These faults are characterized by displacements up to a few hundreds of meters.

The La Forchetta quarry is located within a stepover between two en-échelon principal fault segments cutting Early Cretaceous shallow-water limestones, which include two alternating facies: 1) peritidal white limestone and 2) oolithic grey limestone. In the quarry and nearby areas, as shown in the conceptual cross-section through the fault zone, we identified three main structural domains (Figs. 4a, 4b, and 4c): principal fault (Domain 1, D1); damage zone (Domain 2, D2); secondary fault zone (Domain 3, D3). We describe the three domains in detail as follows.

4.2. Principal fault (D1)

The principal fault (Figs. 4a and 5a) accommodates ∼1500 m of throw and concentrates most shear deformation through ∼1 m thick fault core, which consists of ultracataclasite and foliated cataclasite (Fig. 5b).

(1) The ultracataclasite, brownish in color, forms discontinuous patches and plagues up to ∼20 cm thick resting above the underlying foliated cataclasite (Fig. 5b). The ultracataclasite occurs only along the principal fault surface (Fig. 3a) and mostly consists of calcite enriched with ∼1.5% of phyllosilicates (mainly illite/smectite) as shown by XRD data (Table S1). The occurrence of phyllosilicates and their role during faulting are beyond the scope of this paper. The boundary between the two fault rocks is sharp and continuous or, alternatively, is marked by small, bulbous protrusions of ultracataclasite into the underlying foliated cataclasite, resembling fluid-like structures (Fig. 7a). Clasts from the foliated cataclasite (between 0.1 and 10 mm in diameter) are dispersed within a ground mass composed by ultrafine-grained material (<0.1 mm in diameter) (Figs. 7a and 8a). Microcrystalline calcite cement pervades the ultracataclasite. The cement is characterized by a low dull red CL color, whereas the clasts and the ultrafine-grained material show black luminescence (Fig. 8b).

(2) The foliated cataclasite is grey and up to ∼80 cm thick (Fig. 7a) and XRD data indicate that consists of 100% calcite (Table S1). The foliation is marked by a series of cataclastic shear zones (Fig. 8c), which encase sigmoids and clasts of host rock affected by extensional microfractures (Fig. 8d). Also in this case, microcrystalline calcite cement pervades the foliated cataclasite. The cement, which represents the groundmass of the foliated cataclasite, and the extensional microfractures are characterized by dull red color under CL light (Fig. 8g).

Within the above-described ultracataclasite and foliated cataclasite, we recognized the following structures:

(1) Extensional fractures filled by fine-grained granular material cutting across the foliated cataclasite, often branching out from the ultracataclasite (Fig. 4a). Based on their geometry, we interpret these filled fractures as granular injections. They form a complex network with sharp boundaries (Figs. 8e and 8f). Randomly oriented, angular to subangular reworked fragments from the ultracataclasite and/or foliated cataclasite are dispersed throughout the ultrafine matrix of the injections defining a massive and unsorted texture (Figs. 8e and 8g). Granular injections have calcite cement with bright red CL color (Fig. 8g).

(2) Type 1 veins (T1 veins) are randomly oriented calcite-filled veins <100 μm thick with discontinuous and/or branching geometry that can be recognized only under CL light (Figs. 8g and 8h). T1 veins often branch out from set 2 injections and cut across both the ultracataclasite and the foliated cataclasite (Fig. 8g). Vein filling is composed by anhedreal and equant calcite crystals <30 μm in diameter with blocky texture (Fig. 8i). Crystals do not show growth competition textures and smooth boundaries form triple junctions textures. No CL zoning is observed within these crystals that have the same bright red CL color of granular injections (Figs. 8g and 8h). The same fluid probably precipitated the calcite of both T1 veins and granular injections.

Type 2 veins (T2 veins) are up to 1 mm thick extensional calcite-filled veins that are often located in steps and rhombshaped pull-apart structures along small Riedel shear fractures (R and P fractures; Fig. 7a). These veins are characterized by sharp boundaries and the filling is composed by subhedral calcite crystals up to 200 μm in size with elongate-blocky textures (Fig. 8j). Growth competition textures (e.g., Hilgers et al., 2004) are common with growth directions perpendicular to vein walls. T2 veins are characterized by no luminescence under CL light and cut across (i.e., postdate) all the previously described structures (Fig. 8g). We recognized T2 veins also within D2 and D3 (Fig. 4a).

(3)

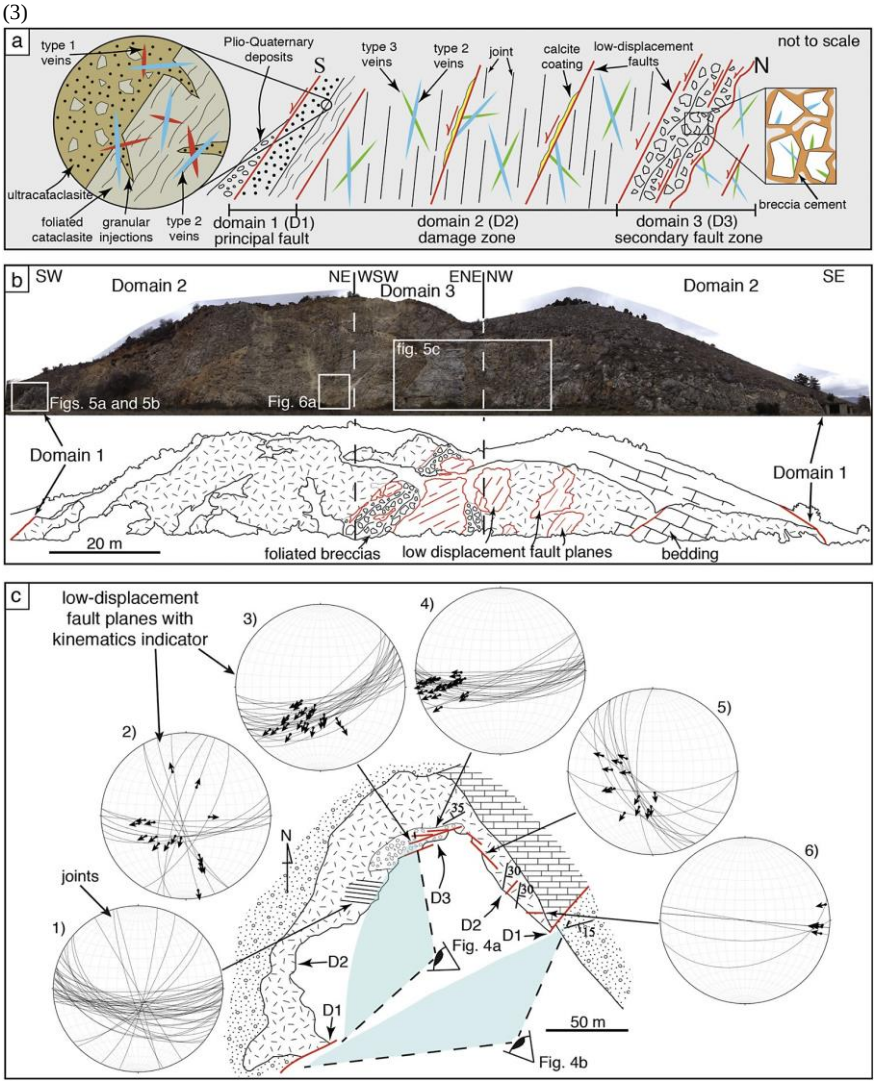

Fig. 4. (a) Simplified conceptual cross-section through the TMF within La Forchetta quarry, showing the crosscutting relationships and three main structural domains: (principal fault, D1; damage zone, D2; secondary fault zone, D3). This figure represents our index reference for what concerns the three studied structural domains, their spatial distribution, and the crosscutting relationships between structures within each domain (see also Table S2). (b) Frontal view of La Forchetta quarry (photograph above and line drawing below), showing exposures of the main structural domains. (c) Simplified structural map of La Forchetta quarry. Schmidt nets (lower hemisphere) show attitude of joints (plot 1) and low displacement faults with related slip vectors (plots from 2 to 6). Quarry location: Latitude 42◦0436N, Longitude 13◦2959E.

4.3. *Damage zone (D2)*

Within the ~60 m thick damage zone (Figs. 4a, 4b, and 5a), deformation is heterogeneously distributed through calcite-filled veins, patches of joints, and low-displacement (<3 m) faults (Fig. 4a). These structures are described as follows.

(1) Type 3 veins (T3 veins) are calcite-filled extensional veins up to 1 mm thick and a few centimeters long (Figs. 7b and 7c). The veins are widespread within the entire damage zone with various orientations. Different sets crosscut each other, creating an intersecting network of calcite filled veins. The resulting texture is a crackle-like breccia similar to those described by Woodcock et al. (2014) in carbonate rocks. The crystals filling these veins are characterized by black luminescence under CL light and by textures similar to T2 veins (D1) (Fig. 8k). In D2, we also recognized T2 veins, which systematically cut across T3 veins. T3 veins are absent in D1 and present in D3 (Fig. 4a).

(2) Joints are frequent in D2 with a wide range of orientations.

The most continuous and penetrative set is subvertical and WNWESE-oriented (plot 1 in Fig. 4c). Joints are not filled and are spaced between 0.5 and 10 cm. They delimit prismatic rock fragments (Fig. 6a) and cut across both T2 and T3 veins (Fig. 4a). Joints are substantially absent in D1.

(3) Low-displacement faults are characterized by two main strikes (N90◦ and N170◦) with slickenfibers indicating oblique-slip and extensional dip-slip motions (plots 2, 5, and 6 in Fig. 4c). Faults and joints are characterized by mutual crosscutting relationships and both cut across T2 and T3 veins (Fig. 4a). Lowdisplacement faults are also present in D3 and absent in D1. Fault surfaces are commonly striated and coated by reddish calcite slickenfibers (Fig. 6b).

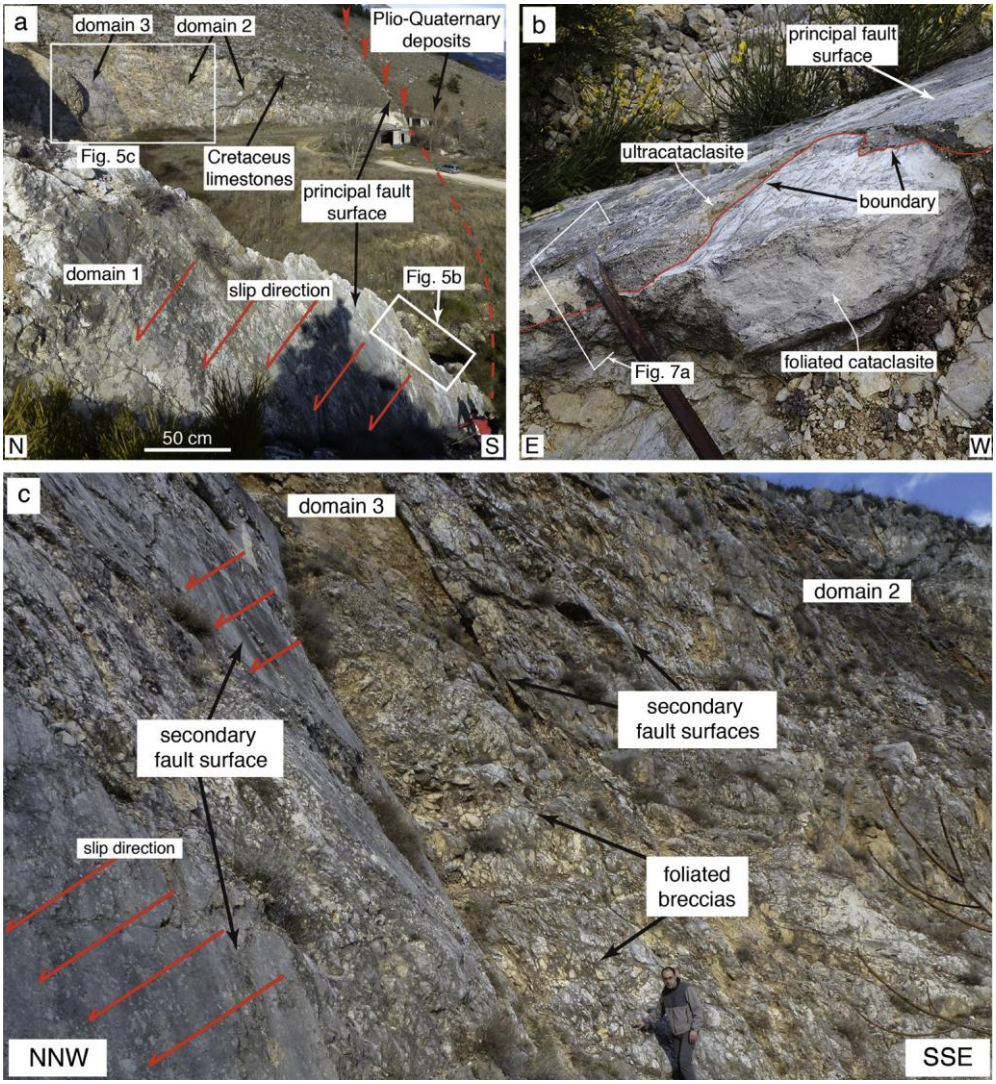

Fig. 5. Large-scale outcrop structures of the Tre Monti Fault within the three structural domains: principal fault (domain 1, D1); damage zone (domain 2, D2); secondary fault zone (domain 3, D3). (a) Overview of the principal fault surface (D1), which juxtaposes Cretaceous carbonate deposits in the footwall and Plio-Pleistocene continental deposits in the hangingwall. (b) Cross-sectional view of the principal fault surface (D1) and related cataclastic fault core, which is ~100 cm thick. The ultracataclasite forms discontinuous patches over the foliated cataclasite. (c) Overview of the secondary fault zone (D3) and damage zone (D2). The secondary fault zone is characterized by optimally exposed fault segments and foliated breccias, which rest above fault surfaces.

4.4. Secondary fault zone (D3)

The secondary fault zone (Figs. 4a, 4b, and 5c) consists of a ~30 m long, ~15 m high, and up to ~5 m thick zone of deformation, accommodating a ~50 m of total throw. The zone contains parallel fault segments encasing the following structures.

(1) The best-exposed fault segment (Fig. 5a) is oriented WNWESE-oriented with reddish calcite slickenfibers indicating rightlateral oblique-slip movements (plots 3 and 4 Fig. 4c).

(2) In D3, we recognized T2 and T3 veins, and joints. T2 veins systematically cut through T3 veins, and T2 and T3 veins are cut by both the fault surfaces and the joints.

(3) Foliated breccias (Fig. 6c) cemented by calcite are present within D3 and rest above striated fault surfaces (Figs. 5c and 6d). The boundaries between breccias and fault surfaces are sharp. Foliations within these breccias consist of undulated, sharp, and striated fault surfaces, which are roughly parallel to low-displacement faults (Figs. 5c and 6d). In places, foliation planes are also characterized by cataclastic textures. Breccias exhibit a chaotic texture (Fig. 7d; classification of Woodcock et al., 2014) with numerous voids. Clasts are randomly oriented, angular to subangular, and their diameter range from <0.1 to 10 cm. Several clasts are characterized by inner crackle breccia textures (Fig. 7d). Within the clasts, we recognized T2 and T3 veins (Fig. 7d). Breccias are cemented by reddish calcite precipitates, which occur in two different generations. Generation 1 cement (G1) consists of blocky to elongateblocky calcite crystals up to 200 μm in diameter (Fig. 8l). This cement fills fractures between clasts. Generation 2 cement (G2) consists of acicular calcite crystals up to 1 mm in length, forming fibrous cement (Fig. 8l). The G2 cement wraps around both carbonate clasts and G1 cement. The breccia is clast-supported, with clasts usually surrounded by G1 and/or G2 cements. "Sealing hiatuses" (sensu Nuriel et al., 2012) between G1 and G2 cements are common (Fig. 8l). Both the G1 and G2 cements show black luminescence under CL light. We synthetize all above-described structures and data in Table S2.

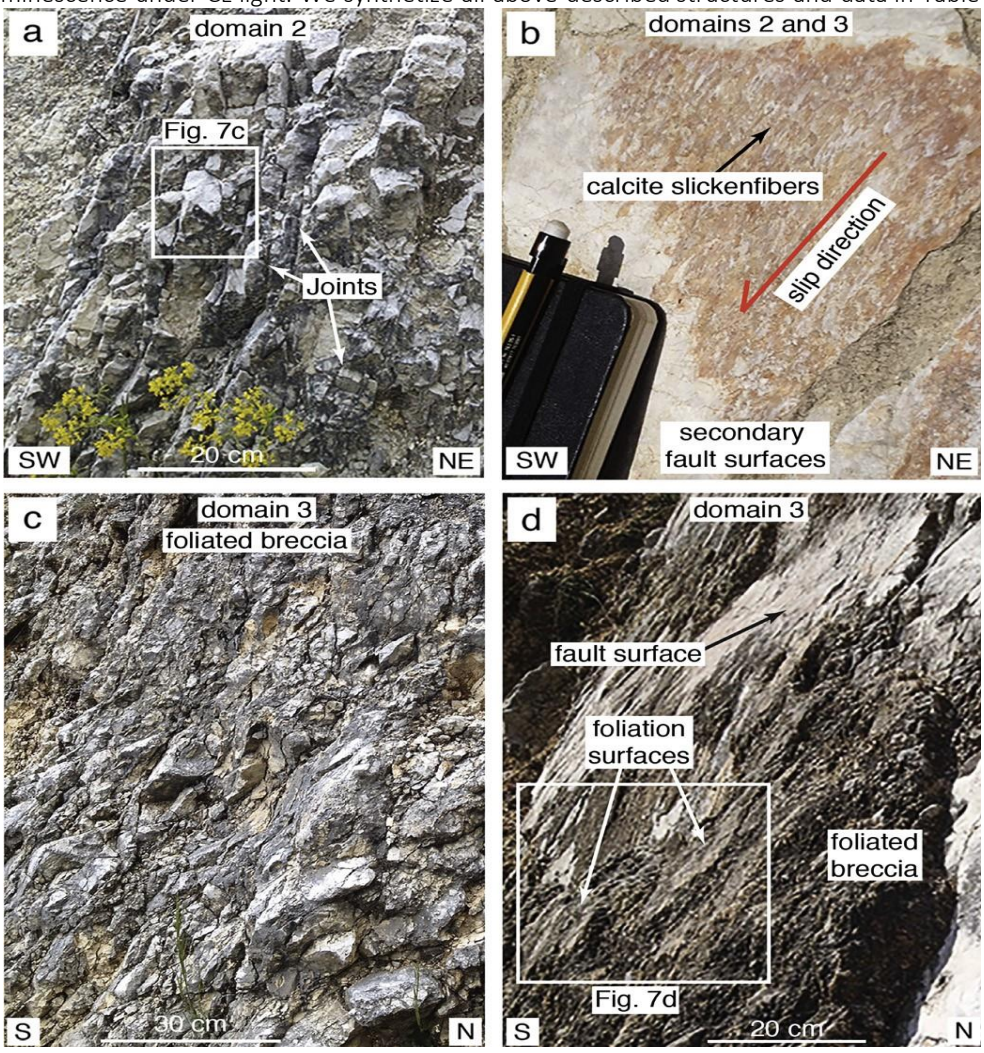

Fig. 6. Mesoscale outcrop structures of the Tre Monti Fault within the damage zone (domain 2, D2) and the secondary fault zone (domain 3, D3). (a) WNW-ESEstriking subvertical joints (D2), which are spaced between 2 and 10 cm. (b) Lowdisplacement fault surface (D2 and D3) coated with reddish calcite slickenfibers. (c) Foliated breccia affected by closely spaced foliation surfaces (D3). (d) Foliated breccias resting above a low-displacement fault surface (D3).

5. Stable isotope data and whole rock geochemistry

5.1. Sampling strategy

To characterize the origin and the temperature of (parental) fluids responsible for the $CaCO_3$ precipitation (veins and cement), we analyzed the C- and O-isotope ($\delta^{13}C$ and $\delta^{18}O$) of 82 samples collected from the TMF domains and nearby rocks (Fig. 9a and Table S3). In detail, we powdered bulk rocks from the ultracataclasite and foliated cataclasite (9 samples, "cataclastic rocks") as well as from the cretaceous host rock sampled outside the fault zone (9 samples, "host rock"). Concerning the cataclastic rocks, we sampled and analyzed bulk volumes, where matrix was the most abundant component, as the host rock-derived clasts were too small to be properly sampled without significant contamination from the surrounding rock. In addition, we used a microdrill equipped with spikes down to 0.3 mm in diameter to extract powder from T2 veins (18 samples, D1, D2 and D3), T3 veins (9 samples, D2 and D3), breccia cements (25 samples, D3), calcite slickenfibers on fault surfaces (4 samples, D2 and D3), and post-orogenic Plio-Quaternary deposits cements in the TMF hangingwall (9 samples). We were not able to sample T1 veins, as they are too thin (<100 μm thick) to be sampled without significant contamination from the surrounding rock. We also determined the whole rock geochemistry of 6 samples from cataclastic rocks (ultracataclasite and foliated cataclasite, D1) and host rock (see detection limits and complete results in Table S4).

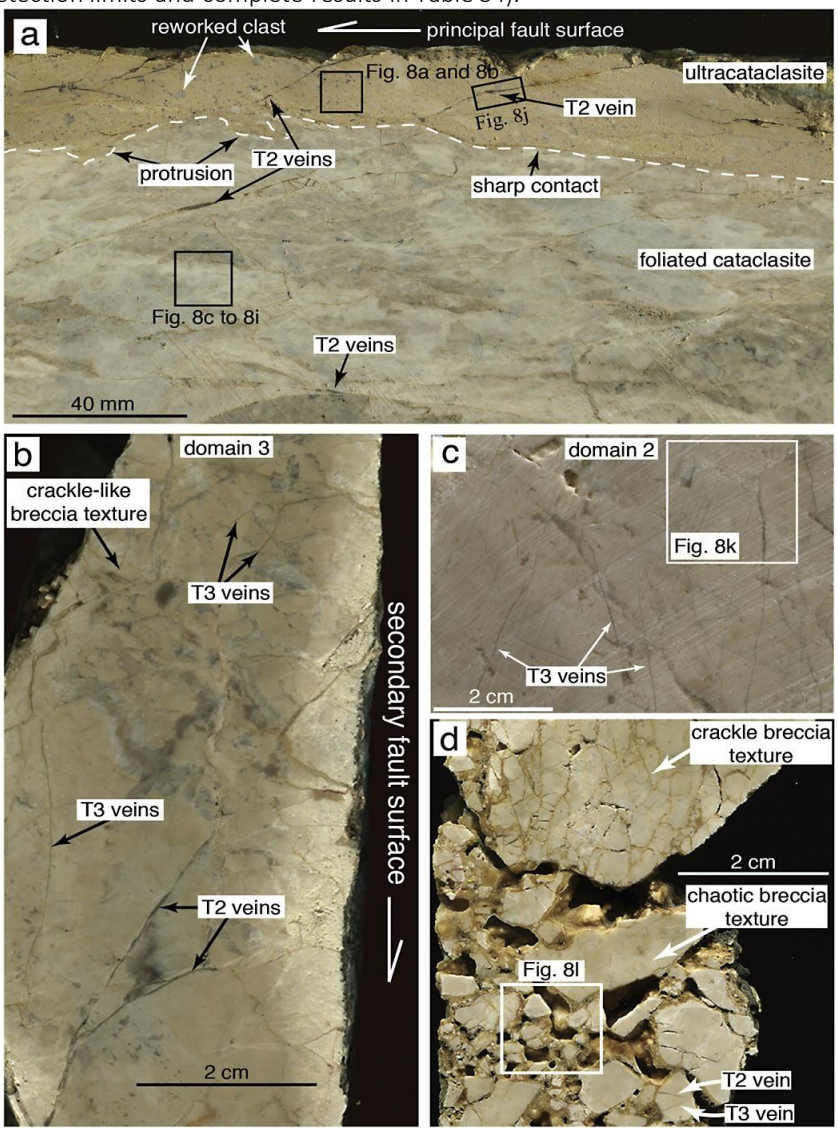

Fig. 7. Mesoscale fault rock structures of the Tre Monti Fault within the three structural domains: principal fault (domain 1, D1); damage zone (domain 2, D2); secondary fault zone (domain 3, D3). (a) High resolution scan of principal fault sample (D1) cut perpendicularly to the fault surface and parallel to slip direction. The boundary between ultracataclasite and foliated cataclasite is sharp and continuous, but often marked by undulations, protrusions, and fluid-like structures. (b) High resolution scan of secondary fault sample (D3) cut perpendicularly to the fault surface and parallel to slip direction characterized by T2 and T3 veins. Note the crackle-like breccia texture created by these veins. (c) High resolution scan of rock sample (D2) including T3 veins. (d) High resolution scan of fault breccia sample (D3) characterized by chaotic texture. Note that the large clast on top is affected by an inner crackle breccia texture. Note also T2 and T3 veins within clasts.

5.2. Results

In Fig. 9a, we distinguished three different end-members characterized by distinct isotope signatures: group 1 (host rock), group 2 (cataclastic rocks and T3 veins), and group 3 (PlioQuaternary deposits cements, breccia cements, T2 veins, and calcite slickenfibers).

Group 1 (host rock): $\delta^{13}C$ and $\delta^{18}O$ values range between $-0.8‰$ and 2.4, and $26‰$ and $31‰$, respectively. Isotope values are in agreement with a marine origin (Sharp, 2007). Moreover, whole rock geochemistry analyses indicate that the host rocks are Ca-rich (close to the calcite composition) and REE (Rare-EarthElements)-poor, with Sr concentrations similar to those of Cretaceous marine carbonates in central Italy as reported by Agosta and Kirschner (2003).

Group 2 (cataclastic rocks and T3 veins): in this group, $\delta^{13}C$ and $\delta^{18}O$ range between $-0.1‰$ and 1.6 and between $21.6‰$ and $24.4‰$, respectively. The average $\delta^{18}O$ value ($23‰$) is lower with respect to that of host rock (by $\sim 5‰$). In addition, whole

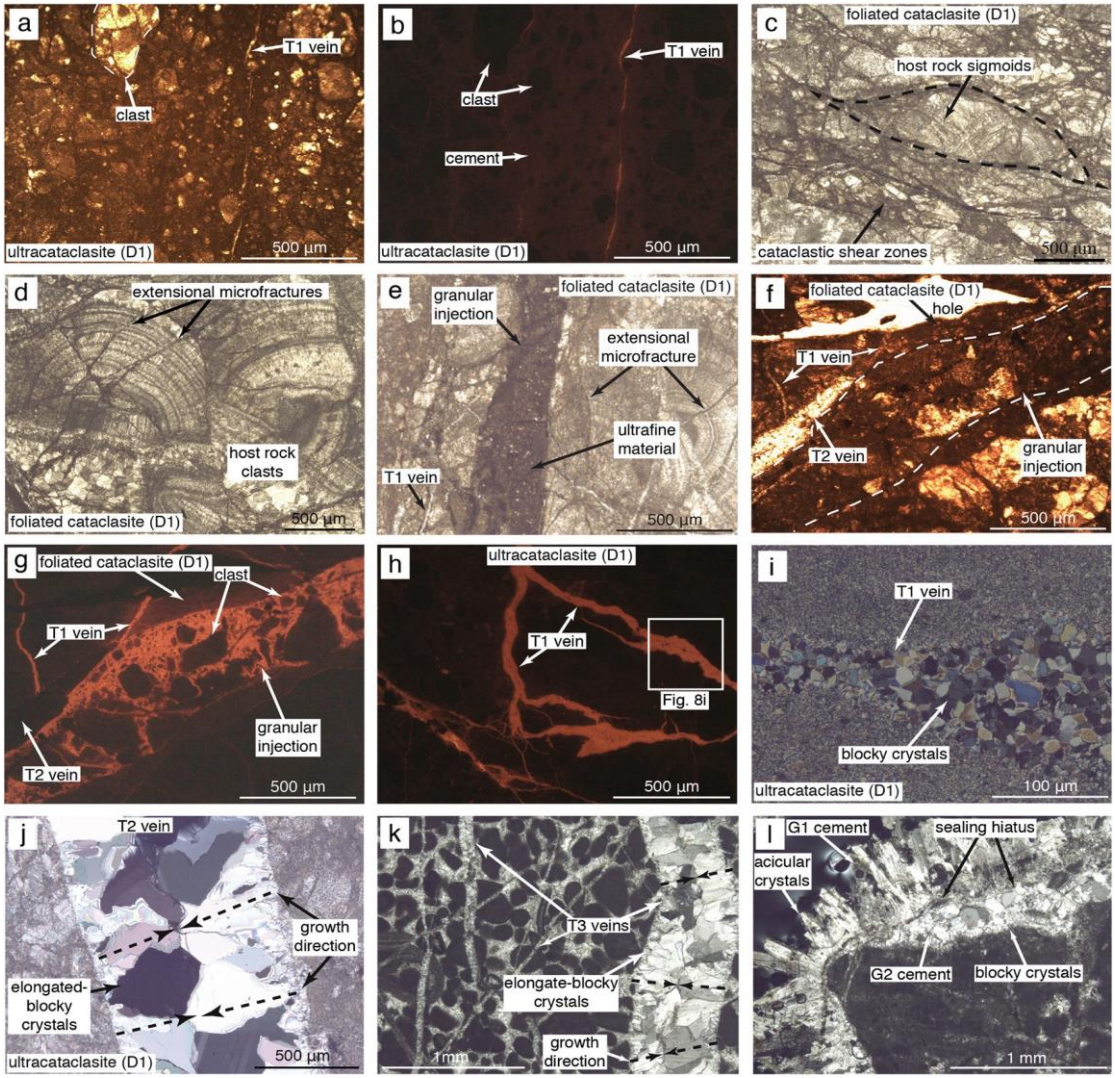

Fig. 8. Microphotographs of the principal fault (Domain 1, D1), damage zone (Domain 2, D2), and secondary fault zone (Domain 3, D3) microstructures taken from thin sections under plane-polarized light (PPL), crossed polarized light (CPL), and/or cathodoluminescence light (CL). (a) Texture of the ultracataclasite (D1). Note the clasts from the foliated cataclasite dispersed within the ultrafine-grained matrix forming the ultracataclasite (PPL). (b) Same as previous microphotograph under CL. Calcite cement has dull red luminescence whereas T1 vein has bright red luminescence. (c) Cataclastic shear zones encasing host rock sigmoids (CPL) within the foliated cataclasite (D1). (d) Host rock clasts within the foliated cataclasite (D1) with extensional microfractures forming a jigsaw puzzle texture (CPL). (e), (f) Granular injections filled by ultrafine material (D1). Note that the injections cut through the foliated cataclasite (PPL). (g) Same as previous microphotograph (f) under CL. Granular injection has bright red luminescence. T1 veins have bright red luminescence and branch out from granular injection. Foliated cataclasite have dull red luminescence. T2 veins have black luminescence. Note the massive and unsorted texture of the granular injection, which cuts across the foliated cataclasite. T2 vein has no luminescence and cuts across the foliated cataclasite, T1 veins, and granular injection. (h) Bright red luminescence of T1 veins under CL light. (i) Vein filling of T1 veins (D1). Anhedral, blocky calcite crystals are characterized by boundaries with triple-junctions (CPL). (j) Elongate-blocky calcite crystals within T2 veins (D1). Arrows indicate growth direction and sense of vein crystals (CPL). (k) T3 veins characterized by elongate-blocky calcite crystals and by mutual crosscutting relationships (D2). Arrows indicate growth direction of vein crystals (CPL). (l) Foliated breccias (D3) with G1 cement characterized by blocky to elongate-blocky calcite crystals, whereas acicular crystals characterize the G2 fibrous cement (CPL). Note the depositional hiatus between G1 and G2 cements

rock geochemistry analyses indicate that the ultracataclasite, when compared with the host rock, is highly enriched in Sr, SiO_2, Al_2O_3, FeO, and REE, and depleted in CaO (Figs. 9b, 9c, and Table S4). The depletion of CaO (∼2 wt%) is accompanied by a depletion (∼1% wt%) in LOI (loss on ignition).

Group 3 (Plio-Quaternary deposits cements, breccia cements, T2 veins, and calcite slickenfibers): in this group $\delta^{13}C$ and $\delta^{18}O$ range between $-3.5‰$ and $-10.2‰$ and between $24.1‰$ and $25.8‰$, respectively. The $\delta^{18}O$ values are characterized by a uniform and narrow range, whereas the $\delta^{13}C$ values are characterized by a broad range.

6. Discussion

6.1. *Fluid sources*

Identifying the fluid sources is critical for the development of a correct model of fluid flow in this and similar tectonic contexts. However, as the exact temperature and the O isotope composition of the parental fluids are unknown, fluid sources cannot be unequivocally determined. To partly solve this problem, we discuss different hypotheses under the reasonable assumptions that the analyzed calcite precipitated in 0–3 km depth and 5◦–100 ◦C temperature ranges as constrained both by geological and by

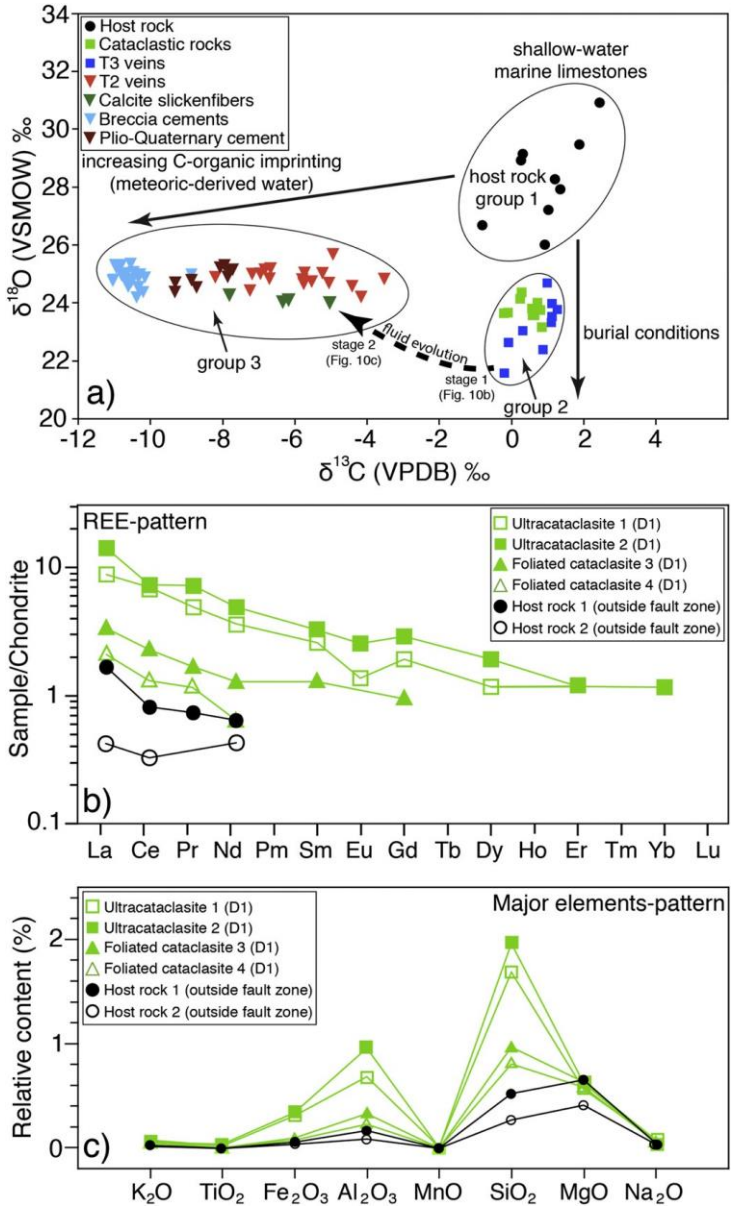

Fig. 9. (a) $\delta^{13}C$ (PDB) versus $\delta^{18}O$ (SMOW) diagram for 82 analyzed samples from various carbonate rocks and mineralizations in the studied fault zone domains and surrounding area. (b) Chondrite-normalized REE-patterns of ultracataclasite and foliated cataclasite (cataclastic rocks, D1) and of host rocks from TMF. Note the significant REE enrichment of the ultracataclasite. (c) Major element pattern of ultracataclasite and foliated cataclasite (cataclastic rocks, D1) and of host rocks from TMF. Note the significant SiO_2, Al_2O_3, Fe_2O_3 enrichment of the ultracataclasite.

organic matter maturity data (Corrado et al., 2010). We hypothesize, in particular, two different fluid end-members, which are responsible for the calcite precipitation of group 2 (cataclastic rocks and T3 veins) and group 3 (breccia cement, T2 veins, and calcite slickenfibers):

(a) Group 2 (cataclastic rocks and T3 veins; Fig. 9a): the $\delta^{18}O$ values of group 2 are characterized by a marked depletion compared with those from the host rocks (group 1). In contrast, $\delta^{13}C$ values are similar to those of the host rocks and marine water (Fig. 9a; Sharp, 2007). The $\delta^{13}C$ values, in particular, are incompatible with calcite precipitation from purely meteoric- and/or groundwater-($\delta^{13}C < -5‰$) as well as from CO_2-rich thermogene ($\delta^{13}C > 5‰$) fluids. In particular, the measured $\delta^{18}O$ values are similar to those measured on calcite veins precipitated from fluids circulating within deep burial settings (e.g., Kirkwood et al., 2001). The observed depletion can be simply explained by a shift from a shallow marine diagenesis (host rock, group 1) towards a deeper one.

The high concentration of Sr, SiO_2, Al_2O_3, Fe_2O_3, and REE (Figs. 9b and 9c) within the ultracataclasite may account for the observed phyllosilicate enrichment, derived from syn-orogenic deposits in the fault hangingwall. However, Sr enrichment (up to 256 ppm) within the ultracataclasite (Table S4) is also consistent with calcite cement precipitation in the presence of highsalinity fluids, such as marine-derived fluids trapped within the syn-orogenic deposits. This hypothesis is also consistent with and would explain the occurrence of phyllosilicates along the main fault, being their fluid transport mediated by marine fluids trapped within the syn-orogenic deposits.

The $\delta^{18}O$ depletion within the cataclastic rocks is interpreted as mainly due to authigenic calcite cement precipitation from an external fluid circulated along the fault core. In particular, the red luminescence of calcite cement and T1 veins within the cataclastic rocks (Figs. 8b, 8g, and 8h) indicates authigenic calcite precipitation from an external fluid in reducing (rich in Mn^{2+}) and deep burial conditions (e.g., Nuriel et al., 2011). However, as we were not able to separate calcite cement from host rock-derived clasts, based on our geochemical data, we cannot exclude a $\delta^{18}O$ overprint related to other processes, such as calcite dissolution/reprecipitation (i.e., pressure-solution mechanism) commonly acting along fault zones. Hence, $\delta^{18}O$ values of calcite cement could be lower than those measured (i.e., $\delta^{18}O$ values of calcite cement is diluted by $\delta^{18}O$ values of host rock derived clasts). A prevalent role of pressure-solution and re-precipitation is probably excluded by the fact that the neoformed calcite should have the same black luminescence of host rock clasts, in contrast to what observed.

The $\delta^{18}O$ and $\delta^{13}C$ values of T3 veins (damage zone, D2) are similar to those of cataclastic rocks (Fig. 9a). This evidence suggests that the same fluid responsible for cement precipitation within cataclastic rocks was also associated with a broader circulation within the damage zone, causing T3 veins precipitation.

All above-reported observations and inferences suggest, as a most likely scenario, group 2 calcite precipitation within a deep burial environment from marine-derived fluids, such as connate fluid trapped within the marine sedimentary succession (foredeep syn-orogenic deposits and carbonate platform deposits). However, our isotope data are also compatible with other complex fluid origins, such as isotopically evoluted (equilibrated with the host rock for $\delta^{13}C$ values) meteoric and/or groundwater-derived fluids infiltrated at depth and mixed with trapped and/or connate fluids.

To calculate the mineralizing fluid temperatures, we assume, in our preferred scenario, calcite precipitation in equilibrium with a marine-like fluid, assuming that this fluid preserved its original commonly occurring within narrow (mm-thick) zones along prinisotopic composition (0 SMOW). Thermally-activated processes,

cipal faults (for instance during seismic slip; Di Toro et al., 2011), may have increased fluid temperatures within the cataclastic fault core (principal fault, D1). For this reason we calculated precipitation temperatures from T3 veins (located within the damage zone, D2, i.e., most likely unaffected by frictional heating), where fluid temperatures may be controlled only by the geothermal gradient at depth. We used the equation of Kele et al. (2015) for inorganic calcite precipitation in the 6◦–95 ◦C temperature range. The calculated precipitation temperatures are in the 60◦ to 75 ◦C range (average value of ∼68 ◦C, Table S2). These values are consistent with the maximum burial depth of 2.5 km calculated for the TMF (assuming a geothermal gradient of 30 ◦C/km typical of immature extensional tectonic setting).

(b) Group 3 (breccia cement, T2 veins, and calcite slickenfibers; Fig. 9a): the $\delta^{13}C$ values lower than $-4‰$ are typical of C-organic imprinting (mostly derived from C_3-type vegetation; Sharp, 2007). This evidence is consistent with a parental fluid that circulated trough organic rich soils before infiltrating within the fault zone. In addition, the $\delta^{13}C$ values are similar to those of groundwater measured in carbonate aquifers in central Apennines (e.g., Falcone et al., 2008). Moreover, the isotope values of T2 veins, calcite slickenfibers, and breccia cements are consistent with those of Plio-Quaternary deposits cements, unequivocally deposited in continental environment. Based on the previous considerations, we conclude that group 3 calcite precipitated from a meteoric-derived fluid that circulated trough organic rich soils and then into carbonates groundwater aquifers before infiltrating within the fault zone. We calculated the mineralizing fluid temperatures considering calcite precipitation in equilibrium with meteoric-derived fluids ($\delta^{18}O$ from −7/−8 SMOW; Sharp, 2007). Results indicate low precipitation temperatures in the 14◦ to 26 ◦C range (Table S2). The calculated temperatures are consistent with in situ temperatures of groundwater aquifers at ≤1 km depth (e.g., Pasquale et al., 2013).

6.2. *Spatio-temporal evolution of fault zone architecture and fluid flow*

The association of different fluid sources with different styles of structural deformation allowed us to reconstruct two different stages of fault zone evolution and fluid circulation during the burial/exhumation history of the shallow portion (<3 km depth) of a carbonate-hosted seismogenic fault. We describe the two stages as follows.

(a) After the compressional phase, characterized by folding and thrusting, the Apennines belt experienced extension, exhumation, and seismicity (Doglioni, 1991; Fig. 10a). In the TMF, based on the crosscutting relationships, the first structures were cataclastic rocks (group 2; D1) within the principal fault and T3 veins in the damage zone (group 2; D2) (Fig. 10b). The isotope data together with the calculated precipitation temperatures (in the 60◦ to 75 ◦C range) indicate calcite precipitation from marinederived fluids at depths <3 km. At these depths, deformation was strongly concentrated along the principal fault (D1), which juxtaposed marine syn-orogenic deposits with pre-orogenic carbonate deposits for a total cumulative displacement >1 km (Fig. 10b). On the other hand, fracturing and veining generated broad and less intense deformation within the damage zone (D2, Fig. 10b). Consequently, marine-derived connate waters trapped within marine syn-orogenic deposits flowed laterally into the principal fault and similar fluids trapped within carbonates deposits flowed into the damage zone (Fig. 10b). Clayey layers within the syn-orogenic deposits may have created low-permeability barriers, which did not allow mixing between connate and external (i.e., meteoricand/or groundwater-derived fluids) fluids. The different luminescence between calcite precipitates within cataclastic rocks (bright and dull) and T3 veins (black) possibly indicate a difference in the redox conditions within precipitation environments and/or slightly different fluid chemistry within the syn-orogenic deposits with respect to that within the carbonate rocks. In this latter case, the principal fault must have provided a permeability barrier to fluid flow toward the damage zone. This setting suggests semiclosed to closed hydrological conditions as documented in other extensional (e.g., Williams et al., 2015) and compressional tectonic settings (e.g., Ghisetti et al., 2001; Kirkwood et al., 2001; Vannucchi et al., 2010).

(b) In the late stage of fault zone development, the exposed portion of the TMF was exhumed by uplift and erosion of the Apennines belt (Galadini et al., 2003). Owing to low confining pressure, deformation was distributed over a broader volume in the damage zone (D2) and in the secondary fault zone (D3), where patches of joints, breccias, T2 veins, and low-displacement faults developed (Fig. 10c). Displacement was no more accommodated only by the principal fault, but also by low-displacement faults.

Isotope values of T2 veins (group 3; D1, D2, and D3), calcite slickenfibers (group 3; D2 and D3), breccia cements (group 3; D3), and black luminescence of these structures indicate calcite precipitation from meteoric- and/or groundwater-derived fluids in the 14◦ to 26 ◦C range typical of depths <1 km. Therefore, we suggest that, during exhumation, the TMF must have intersected shallow (<1 km depth) groundwater aquifers connected with the Earth's surface so that meteoric-derived fluids infiltrated downward into the fault zone (Fig. 10c) through high-permeability structural conduits (i.e., breccia lenses and joints). The large variation in $\delta^{13}C$ isotope values suggests different degrees of organic carbon contamination or variable organic carbon contamination within the aquifer during multiple events of fluid infiltrations into the fault zone. Similar scenarios have been documented in other carbonate fault zones in the same region (e.g., Agosta and Kirschner, 2003) and in other tectonic settings (e.g., Menzies et al., 2014), also in connection with seismic sequences (Amoruso et al., 2011; Doglioni et al., 2014).

6.3. *Fluid involvement in the seismic cycle*

In this section, we discuss a model for fluid circulation, fluid pressure fluctuations, and fluid redistribution during concurrent exhumation and seismic activity within the shallow portion (≤3 km depth) of active fault zones in carbonate rocks, such as the TMF.

(a) Inter-seismic phase: The high permeability networks of fractures and breccias of the TMF allowed the maintenance of hydrostatic fluid pressure up to a depth of ∼3 km within criticallystressed faults (e.g., Townend and Zoback, 2000). Fluid pressure was essentially at hydrostatic value between ∼3 km and ∼1 km depth and at depth ≤1 km within the whole fault zone (Figs. 10b and 10c).

(b) Co-seismic phase: crackle and chaotic breccia textures suggest that the TMF slipped seismically with episodic events of coseismic dilatancy and implosive brecciation within dilational jogs associated with a rapid fluid depressurization (e.g., Sibson, 2000; Woodcock et al., 2014). Cataclasis and shearing may have been either synchronous with co-seismic slip or associated with aseismic creep during interseismic periods (e.g., Stünitz et al., 2010). We propose that extensional fractures and crackle-like brecciation within the damage zone between ∼3 km and ∼1 km depth (D2 and D3; Fig. 10b) and within the whole fault zone at depth ≤1 km (D1, D2, and D3; Fig. 10c) occurred by co-seismic dilatancy at hydrostatic fluid pressure both by rapid tensile pulses propagation (e.g., Ben-Zion and Shi, 2005) and by dilatancy along fault dilational jogs (e.g., Sibson, 2000) rather than by hydrofracturing at near-lithostatic fluid pressure. Dilational jogs commonly develop along strongly undulated fault surfaces, such as those of the secondary fault zone (Fig. 5c). As tensile strength is small for most sedimentary rocks (1–10 MPa), extensional fracturing and dilatancy can occur down to ∼3–4 km depth at hydrostatic fluid pressure (e.g., Sibson, 2000). Even if overpressured fluids were generated at depths of ∼5–10 km (e.g., Miller et al., 2004; Haney et al., 2005; Di Luccio et al., 2010), these overpressures could not have been sustained during their upward propagation within high permeability fracture networks and breccias of shallow fault zones (Townend and Zoback, 2000). Thus, hydrofracturing was improbable at shallow crustal depths (≤3 km). Immediately after co-seismic dilatancy, the fluid pressure dropped toward subhydrostatic values into newly created extensional fractures allowing the suction of fluids into fractures, CO_2 partial pressure drop and exsolution, and calcite precipitation from a suprasaturated solution (e.g., Uysal et al., 2009;

Figs. 10b and 10c). Crosscutting relationships and isotopes data from TMF suggest multiple events of earthquake-related dilatancy (i.e., extensional fracturing and brecciation), earthquake-related fluid circulation, and calcite precipitation.

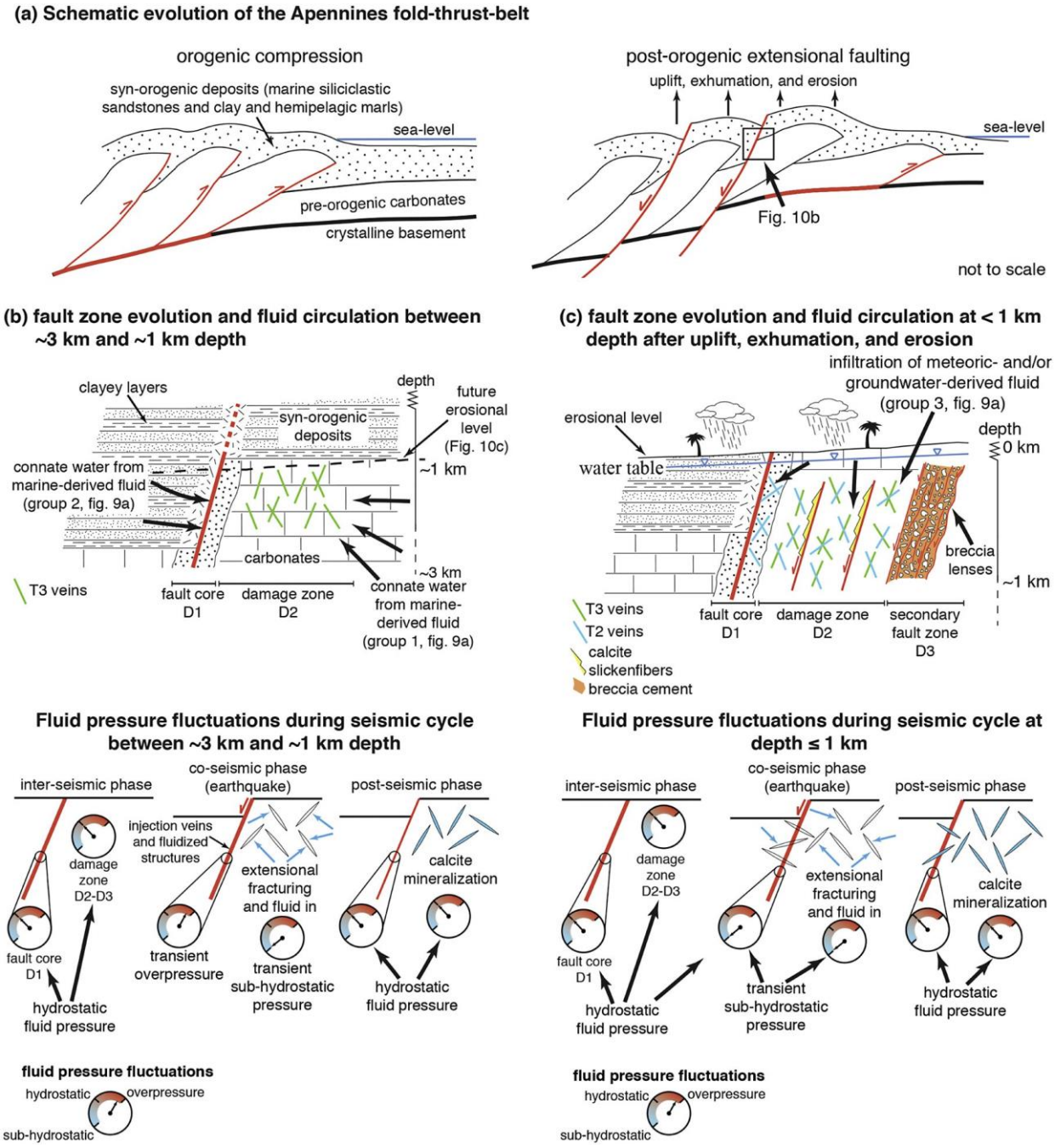

Fig. 10. Cartoon showing the conceptual model for the evolution of a shallow (≤3 km) extensional fault zone and seismic-related fluid circulation. (a) Burial-exhumation history of the Apennines belt involving compression and post-collisional extension. (b) In the first stage of fault zone evolution, deformation and fault displacement are concentrated along the principal fault surface (D1), whereas less intense deformation is distributed within the damage zone (D2). The isotope trend in the $\delta^{18}O$–$\delta^{13}C$ space indicates that calcite prevalently precipitated from marine-derived fluids (brines and/or connate waters) between ~3 km and ~1 km depth and at temperature of ~68◦C. At these depths, during co-seismic dilation, fluid pressure instantaneously dropped at sub-hydrostatic pressure conditions within newly created dilatant fractures occurring in the damage zone (D2). This process led to calcite precipitation and mineralization. At the same time, localized and transient suprahydrostatic pressure condition were generated along the principal fault surface (D1). After the co-seismic phase, fluids regained hydrostatic pressure conditions. (c) In the second stage of fault zone evolution, deformation and fault displacement are distributed within the damage zone (D2) and the secondary fault zone (D3). The isotope trend in the $\delta^{18}O$–$\delta^{13}C$ space indicates that calcite precipitated from meteoric- and/or groundwater-derived fluids at depths ≤1 km and temperatures below 35 ◦C. At these depths, during co-seismic dilation, fluid pressure instantaneously dropped at subhydrostatic pressure conditions within newly created dilatant fracture in the whole fault zone (D1–D2–D3). This process led to calcite precipitation and mineralization. No evidence of localized and transient suprahydrostatic pressure conditions are present. After the co-seismic phase, fluids regained hydrostatic pressure conditions.

However, we found evidence indicating that transient overpressures were only localized into the principal fault (D1) when the fault was active between ∼3 km and ∼1 km depth (Fig. 10b). Granular injections show texture of injection veins similar to those described by Lin (2011), indicating that fluid and ultrafine granular material became fluidized to form a solid–liquid system, which was squeezed into the complex network of extensional hydrofractures created by overpressured fluids. Moreover, we interpret fluid-like structures (Fig. 7a) similar to those found at smaller scales in the TMF by Smith et al. (2011) as the result of fluidization of granular material that probably occurred by overpressured fluid release. In addition, calcite crystal textures in T1 veins indicate very high calcite precipitation rate (e.g., Boullier et al., 2004). This is due to large CO_2 pressure drop and exsolution as, at low temperatures (<100 ◦C), the larger the CO_2 pressure drop and exsolution, the higher the calcite precipitation rate. Large pressure drops likely occurred during fall from suprahydrostatic fluid pressure (i.e., nearlithostatic) to hydrostatic fluid pressure within newly created hydrofractures.

(c) Post-seismic phase: After co-seismic dilatancy, fluids were passively redistributed at hydrostatic pressure level through the newly created network of high permeable extensional fractures and breccias (Figs. 10b and 10c). Microstructures of calcite filled veins indicate that extensional fractures remained open at hydrostatic pressure conditions until sealing occurred. Calcite filling is characterized by subhedral crystals with growth competition textures, indicating that crystals slowly precipitated into fluid-filled and open spaces with continuous advection of suprasaturated solution (e.g., Hilgers et al., 2004). Estimated growth rates of natural calcite crystals in tectonic veins precipitated at non-equilibrium conditions range between 10^{-1} and 10^{-2} mm/a (Uysal et al., 2009; Frery et al., 2015). Veins from TMF are only up to 1 mm wide, indicating that they may have been sealed in a few years or months and even less time for thinner veins. Localized and transient fluid pressure (e.g., Hadizadeh et al., 2012) could not have maintained extensional fractures open for such times.

7. Conclusions

We integrated geological mapping and structural analyses together with cathodoluminescence, mineralogical, and geochemical investigations to propose, from a single case history, a conceptual model of seismic fault zone evolution. In the studied case, the stratigraphic-structural setting and burial-exhumation history involved the presence of different types of geofluids (i.e., marineand meteoric-derived), which have actively or passively assisted the seismic cycle. Between ∼3 km and ∼1 km depths and temperatures between 60 and 75 ◦C, prevalently marine-derived fluids trapped within syn-orogenic deposits and carbonate rocks in the hangingwall and footwall, respectively, circulated within the fault zone. Semi-closed hydrological circulation, created by lowpermeability barriers within the syn-orogenic deposits (i.e., clayey layers), did not allow substantial mixing with meteoric-derived fluid. During co-seismic dilatancy, fluid pressure shifted toward sub-hydrostatic values in the damage zone and toward an overpressure state along the principal fault, where overpressured fluids actively assisted the co-seismic slip promoting hydrofracturing and granular fluidization. During the post-seismic phase, fluids were passively re-distributed at hydrostatic pressure. With the progressive exhumation toward depths ≤1 km, the hydrological circulation became open due to the formation of high permeability conduits (i.e., high permeability breccia lenses). Meteoric-derived fluids infiltrated and circulated within groundwater aquifers and then into the fault zone at temperatures <30 ◦C. At these depths, fluid pressure shifted from subhydrostatic to hydrostatic values during co-seismic and post-seismic phases, respectively, without fluid overpressure occurrences. We assess that the proposed model of seismic fluid–fault interaction can be valid elsewhere as the stratigraphic and tectonic setting of the Central Apennines is similar to other seismically active fold-thrust belts characterized by later extension and exhumation. We point out, in particular, the role played by low-permeability compartments that can modulate the type of fluids infiltrating into the fault zone at various levels of exhumation.

Acknowledgements

Financial support from PRIN2010/11 (Project 20107ESMX9 “Crisi e ripresa di sistemi carbonatici e potenziale per la formazione di reservoir: i ruoli di clima, tettonica e magmatismo”) and Progetti di Ateneo (Sapienza) 2012 and 2014 led by Carlo Doglioni and Eugenio Carminati is acknowledged. Editor and reviewers are thanked for their constructive comments and editorial efforts. Francesca Castorina, Andrea Cavallo, Cristiano Collettini, Giulio Di Toro, Michele Fondriest, Shalev Siman-Tov, Steve Smith, and Fabio Trippetta are thanked for fruitful discussions. Domenico Mannetta is thanked for thin section preparation. Ilaria Baneschi and Simone Vezzoni are thanked for help during sample preparation and isotope analyses. Federico Zorzi and Giulio Di Toro are thanked for fruitful discussions and XRD analyses. Alessio Fazioli and Luca Rubeis are thanked for help during fieldwork.

Appendix A. Supplementary material

Supplementary material related to this article can be found online at http://dx.doi.org/10.1016/j.epsl.2016.06.042.

References

Agosta, F., Kirschner, D.L., 2003. Fluid conduits in carbonate-hosted seismogenic normal faults of central Italy. J. Geophys. Res. 108, 2221. http://dx.doi.org/10.1029/ 2002JB002013.

Amoruso, A., Crescentini, L., Petitta, M., Rusi, S., Tallini, M., 2011. Impact of the 6 April 2009 L'Aquila earthquake on groundwater flow in the Gran Sasso carbonate aquifer, Central Italy. Hydrol. Process. 25, 1754–1764. http://dx.doi.org/ 10.1002/hyp.7933.

Ben-Zion, Y., Shi, Z., 2005. Dynamic rupture on a material interface with spontaneous generation of plastic strain in the bulk. Earth Planet. Sci. Lett. 236, 486–496. http://dx.doi.org/10.1016/j.epsl.2005.03.025.

Benedetti, L., Manighetti, I., Gaudemer, Y., Finkel, R., Malavieille, J., Pou, K., Maurice, A., Aumaitre, G., Bourlès, D., Keddadouche, K., 2013. Earthquake synchrony and clustering on Fucino faults (Central Italy) as revealed from in situ ^{36}Cl exposure dating. J. Geophys. Res. 118, 4948–4974. http://dx.doi.org/10.1002/jgrb.50299.

Boullier, A.M., Fujimoto, K., Ohtani, T., Roman-Ross, G., Lewin, E., Ito, H., Pezard, P., Ildefonse, B., 2004. Textural evidence for recent co-seismic circulation of fluids in the Nojima fault zone, Awaji island, Japan. Tectonophysics 378, 165–181. http://dx.doi.org/10.1016/j.tecto.2003.09.006.

Cavinato, G.P., Carusi, C., Dall'Asta, M., Miccadei, E., Piacentini, T., 2002. Sedimentary and tectonic evolution of Plio-Pleistocene alluvial and lacustrine deposits of Fucino Basin (central Italy). Sediment. Geol. 148, 29–59. PII: S00370738(01)00209-3.

Chen, J., Yang, X., Ma, S., Spiers, C.J., 2013. Mass removal and clay mineral dehydration/rehydration in carbonate-rich surface exposures of the 2008 Wenchuan Earthquake fault: geochemical evidence and implications for fault zone evolution and coseismic slip. J. Geophys. Res. 118, 474–496. http://dx.doi.org/10.1002/ jgrb.50089.

Chiaraluce, L., 2012. Unravelling the complexity of Apenninic extensional fault systems: a review of the 2009 L'Aquila earthquake (Central Apennines, Italy). J. Struct. Geol. 42, 2–18. http://dx.doi.org/10.1016/j.jsg.2012.06.007.

Corrado, S., Aldega, L., Zattin, M., 2010. Sedimentary vs. tectonic burial and exhumation along the Apennines (Italy). In: Beltrando, M., Peccerillo, A., Mattei, M., Conticelli, S., Doglioni, C., (Eds.), The Geology of Italy. J. Virtual Explorer 36, 1–37. http://dx.doi.org/10.3809/jvirtex.2010.00232. Electronic Edition, paper 15.

Cosentino, D., Cipollari, P., Marsili, P., Scrocca, D., 2010. Geology of the central Apennines: a regional review. In: Beltrando, M., Peccerillo, A., Mattei, M., Conticelli, S., Doglioni, C., (Eds.). J. Virtual Explorer 36, 1–36. http://dx.doi.org/10.3809/ jvirtex.2010.00223, paper 12.

Cox, S.F., 1995. Faulting processes at high fluid pressures: an example of fault valve behavior from the Wattle Gully Fault, Victoria, Australia. J. Geophys. Res. 100, 12841–12859.

Di Luccio, F., Ventura, G., Di Giovambattista, R., Piscini, A., Cinti, F.R., 2010. Normal faults and thrusts reactivated by deep fluids: the 6 April 2009 M_w 6.3 L'Aquila earthquake, central Italy. J. Geophys. Res. 115, 1–15. http://dx.doi.org/ 10.1029/2009JB007190.

Di Toro, G., Han, R., Hirose, T., De Paola, N., Nielsen, S., Mizoguchi, K., Ferri, F., Cocco, M., Shimamoto, T., 2011. Fault lubrication during earthquakes. Nature 471, 494–498. http://dx.doi.org/10.1038/nature09838.

Doglioni, C., 1991. A proposal for the kinematic modelling of W-dipping subductions; possible applications to the Tyrrhenian–Apennines system. Terra Nova 3, 423–434.

Doglioni, C., Barba, S., Carminati, E., Riguzzi, F., 2014. Fault on-off versus coseismic fluids reaction. Geosci. Front. 5, 767–780. http://dx.doi.org/10.1016/ j.gsf.2013.08.004.

Falcone, R.A., Falgiani, A., Parisse, B., Petitta, M., Spizzico, M., Tallini, M., 2008. Chemical and isotopic (δ^{18}O‰, δ^{2}H‰, δ^{13}C‰, ^{222}Rn) multi-tracing for groundwater conceptual model of carbonate aquifer (Gran Sasso INFN underground laboratory-central Italy). J. Hydrol. 357, 368–388. http://dx.doi.org/10.1016/j.jhydrol.2008.05.016.

Frery, E., Gratier, J.P., Ellouz-Zimmerman, N., Loiselet, C., Braun, J., Deschamps, P., Blamart, D., Hamelin, B., Swennen, R., 2015. Evolution of fault permeability during episodic fluid circulation: evidence for the effects of fluid–rock interactions from travertine studies (Utah–USA). Tectonophysics 651, 121–137. http://dx.doi.org/10.1016/j.tecto.2015.03.018.

Galadini, F., Messina, P., Giaccio, B., Sposato, A., 2003. Early uplift history of the Abruzzi Apennines (central Italy): available geomorphological constraints. Quat. Int. 101–102, 125–135. http://dx.doi.org/10.1016/S1040-6182(02)00095-2.

Galli, P., Galadini, F., Pantosti, D., 2008. Twenty years of paleoseismology in Italy.
Earth-Sci. Rev. 88, 89–117. http://dx.doi.org/10.1016/j.earscirev.2008.01.001.

Ghisetti, F., Kirschner, D.L., Vezzani, L., Agosta, F., 2001. Stable isotope evidence for contrasting paleofluid circulation in thrust faults and normal faults of the central Apennines, Italy. J. Geophys. Res. 106, 8811–8825.

Hadizadeh, J., Mittempergher, S., Gratier, J.P., Renard, F., Di Toro, G., Richard, J., Babaie, H.A., 2012. A microstructural study of fault rocks from the SAFOD: implications for the deformation mechanisms and strength of the creeping segment of the San Andreas Fault. J. Struct. Geol. 42, 246–260. http://dx.doi.org/10.1016/ j.jsg.2012.01.011.

Haney, M.M., Snieder, R., Sheiman, J., Losh, S., 2005. Geophysics: a moving fluid pulse in a fault zone. Nature 437, 46. http://dx.doi.org/10.1038/437046.

Hickman, S., Sibson, R., Bruhn, R., 1995. Introduction to special section: mechanical involvement of fluids in faulting. J. Geophys. Res. 100, 12831–12840.

Hilgers, C., Dilg-Gruschinski, K., Urai, J.L., 2004. Microstructural evolution of syntaxial veins formed by advective flow. Geology 32, 261–264. http://dx.doi.org/ 10.1130/G20024.1.

Kele, S., Breitenbach, S.F.M., Capezzuoli, E., Nele Meckler, A., Ziegler, M., Millan, I.M., Kluge, T., Deák, J., Hanselmann, K., John, C.M., Yan, H., Liu, Z., Bernasconi, S.M., 2015. Temperature dependence of oxygen- and clumped isotope fractionation in carbonates: a study of travertines and tufas in the 6–95 ◦C temperature range. Geochim. Cosmochim. Acta 168, 172–192. http://dx.doi.org/10.1016/j.gca.2015.06.032.

Kirkwood, D., Savard, M.M., Chi, G., 2001. Microstructural analysis and geochemical vein characterization of the Salinic event and Acadian Orogeny: evaluation of the hydrocarbon reservoir potential in eastern Gaspé. Bull. Can. Pet. Geol. 49, 262–281.

Lin, A., 2011. Seismic slip recorded by fluidized ultracataclastic veins formed in a coseismic shear zone during the 2008 M_w 7.9 Wenchuan earthquake. Geology 39, 547–550. http://dx.doi.org/10.1130/G32065.1.

Malagnini, L., Lucente, F.P., De Gori, P., Akinci, A., Munafo, I., 2012. Control of pore fluid pressure diffusion on fault failure mode: insights from the 2009 L'Aquila seismic sequence. J. Geophys. Res. 117, B05302. http://dx.doi.org/10.1029/ 2011JB008911.

Menzies, C.D., Teagle, D.A., Craw, D., Cox, S.C., Boyce, A.J., Barrie, C.D., Roberts, S., 2014. Incursion of meteoric waters into the ductile regime in an active orogen. Earth Planet. Sci. Lett. 399, 1–13. http://dx.doi.org/10.1016/j.epsl.2014.04.046.

Miller, S.A., Collettini, C., Chiaraluce, L., Cocco, M., Barchi, M., Kaus, B.J.P., 2004. Aftershocks driven by a high-pressure CO_2 source at depth. Nature 427, 724–727. http://dx.doi.org/10.1038/nature02251.

Morewood, N., Roberts, G.P., 2000. The geometry, kinematics and rates of deformation within an en échelon normal fault segment boundary, central Italy. J. Struct. Geol. 22, 1027–1047. PII: S0191-8141(00)00030-4.

Nuriel, P., Rosenbaum, G., Uysal, I.T., Zhao, J.-X., Golding, S.D., Weinberger, R., Karabacak, V., Avni, Y., 2011. Formation of fault-related calcite precipitates and their implications for dating fault activity in the East Anatolian and Dead Sea fault zones. In: Fagereng, Å., et al., (Eds.), Geology of the Earthquake Source: A Volume in Honour of Rick Sibson. Geol. Soc. (Lond.) Spec. Publ. 359, 229–248. http://dx.doi.org/10.1144/SP359.13.

Nuriel, P., Weinberger, R., Rosenbaum, G., Golding, S.D., Zhao, J.-X., Uysal, I.T., BarMatthews, M., Gross, M.R., 2012. Timing and mechanism of late-Pleistocene calcite vein formation across the Dead Sea Fault Zone, northern Israel. J. Struct. Geol. 36, 43–54. http://dx.doi.org/10.1016/j.jsg.2011.12.010.

Pasquale, V., Chiozzi, P., Verdoya, M., 2013. Evidence for thermal convection in the deep carbonate aquifer of the eastern sector of the Po Plain, Italy. Tectonophysics 594, 1–12. http://dx.doi.org/10.1016/j.tecto.2013.03.011.

Patacca, E., Scandone, P., Di Luzio, E., Cavinato, G.P., Parotto, M., 2008. Structural architecture of the central Apennines: interpretation of the CROP 11 seismic profile from the Adriatic coast to the orographic divide. Tectonics 27, tc3006. http://dx.doi.org/10.1029/2005tc001917.

Rowe, C.D., Griffith, W.A., 2015. Do faults preserve a record of seismic slip: a second opinion. J. Struct. Geol. 78, 1–26. http://dx.doi.org/10.1016/j.jsg.2015.06.006.

Sharp, Z., 2007. Principles of Stable Isotope Geochemistry. Pearson Prentice Hall. 344 pp.

Sibson, R.H., 2000. Fluid involvement in normal faulting. J. Geodyn. 29, 469–499. PII: S0264-3707(99)00042-3.

Sibson, R.H., 2014. Earthquake rupturing in fluid-overpressured crust: how common? Pure Appl. Geophys. 171, 2867–2885. http://dx.doi.org/10.1007/ s00024-014-0838-3.

Smith, S.A.F., Billi, A., Di Toro, G., Spiess, R., 2011. Microstructures of principal slip zones in limestones, and implications for the seismic cycle (Tre Monti fault, central Appennines, Italy). Pure Appl. Geophys. 168, 2365–2393. http://dx.doi.org/10.1007/s00024-011-0301-7.

Stiros, S., 1995. Unexpected shock rocks an 'aseismic' area. Eos 76, 513–519. http://dx.doi.org/10.1029/95EO00316.

Stünitz, H., Keulen, N., Hirose, T., Heilbronner, R., 2010. Grain size distribution and microstructures of experimentally sheared granitoid gouge at coseismic slip rates–Criteria to distinguish seismic and aseismic faults? J. Struct. Geol. 32, 59–69. http://dx.doi.org/10.1016/j.jsg.2009.08.002.

Thomson, S.N., Brandon, M.T., Reiners, P.W., Zattin, M., Isaacson, P.J., Balestrieri, M.L., 2010. Thermochronologic evidence for orogen-parallel variability in wedge kinematics during extending convergent orogenesis of the northern Apennines, Italy. Geol. Soc. Am. Bull. 122, 1160–1179. http://dx.doi.org/10.1130/B26573.1.

Townend, J., Zoback, M.D., 2000. How faulting keeps the crust strong. Geology 28, 399–402. http://dx.doi.org/10.1130/0091-7613.

Uysal, I.T., Feng, Y., Zhao, J.X., Isik, V., Nuriel, P., Golding, S.D., 2009. Hydrotermal CO_2 degassing in seismically active zones during the Late Quaternary. Chem. Geol. 265, 442–454. http://dx.doi.org/10.1016/j.chemgeo.2009.05.011.

Vannucchi, P., Remitti, F., Bettelli, G., Boschi, C., Dallai, L., 2010. Fluid history related to the early Eocene–middle Miocene convergent system of the Northern Apennines (Italy): constraints from structural and isotopic studies. J. Geophys. Res. 115, 1978–2012. http://dx.doi.org/10.1029/2009JB006590.

Ventura, G., Di Giovambattista, R., 2013. Fluid pressure, stress field and propagation style of coalescing thrusts from the analysis of the 20 May 2012 ML 5.9 Emilia earthquake (Northern Apennines, Italy). Terra Nova 25, 72–78. http:// dx.doi.org/10.1111/ter.12007.

Williams, R.T., Goodwin, L.B., Mozley, P.S., Beard, B.L., Johnson, C.M., 2015. Tectonic controls on fault zone flow pathways in the Rio Grande rift, New Mexico, USA. Geology 43, 723–726. http://dx.doi.org/10.1130/G36799.1.

Woodcock, N.H., Miller, A.V.M., Woodhouse, C.D., 2014. Chaotic breccia zones on the Pembroke Peninsula, south Wales: evidence for collapse into voids along dilational faults. J. Struct. Geol. 69, 91–107. http://dx.doi.org/10.1016/ j.jsg.2014.09.019.